

# DMAPS: a fully depleted monolithic active pixel sensor - analog performance characterization

M. Havránek<sup>\*, \*\*</sup>, T. Hemperek, H. Krüger, Y. Fu, L. Germic,  
T. Kishishita, T. Obermann and N. Wermes

*Physikalisches Institut, Universität Bonn  
Nußallee 12, 53115 Bonn, Germany<sup>†</sup>*

## Abstract

Monolithic Active Pixel Sensors (MAPS) have been developed since the late 1990s based on silicon substrates with a thin epitaxial layer (thickness of 10-15  $\mu\text{m}$ ) in which charge is collected on an electrode, albeit by disordered and slow diffusion rather than by drift in a directed electric field. As a consequence, the signal is small ( $\approx 1000 e^-$ ) and the radiation tolerance is much below the LHC requirements by factors of 100 to 1000. In this paper we present the development of a fully Depleted Monolithic Active Pixel Sensors (DMAPS) based on a high resistivity substrate allowing the creation of a fully depleted detection volume. This concept overcomes the inherent limitations of charge collection by diffusion in the standard MAPS designs. We present results from a test chip EPCB01 designed in a commercial 150 nm CMOS technology. The technology provides a thin ( $\sim 50 \mu\text{m}$ ) high resistivity n-type silicon substrate as well as an additional deep p-well which allows to integrate full CMOS circuitry inside the pixel. Different matrix types with several variants of collection electrodes have been implemented. Measurements of the analog performance of this first implementation of DMAPS pixels will be presented.

*Keywords:* CMOS, MAPS, pixel detector, front-end electronics.

---

\* Corresponding author

Email: miroslav.havranek@cern.ch

\*\* Now at FNSPE, Czech Technical University, Břehová 7, 115 19 Praha, Czech Republic

† Work supported by the German Deutsche Forschungsgemeinschaft DFG under contract WE 976/4-1

# 1 Introduction

Monolithic Active Pixel Sensors (MAPS) have been proposed [1], [2] as tracking detectors for particle physics experiments allowing high spatial resolution and a superior material budget compared to hybrid pixel detectors [3]. Unlike the latter, MAPS integrate both sensor and front-end (FE) electronics in a single silicon chip and thus do not require costly and often difficult chip-to-sensor interconnection. However, standard MAPS pixel sensors have two drawbacks which limit their area of application: First, in a standard CMOS process the common implant well configuration does not allow to use both transistor types (NMOS and PMOS) in the pixel area, thus severely limiting the complexity of the electronics circuitry. To overcome this limitation, an additional implant must be added in the technology to isolate the electronics from the charge collection nodes as introduced for example in [4] and [5]. Second, the collection of charge released from a particle or radiation is accomplished by diffusion rather than by drift in an electric field and is hence slow, severely limiting the achievable time resolution (e.g. for time stamping) and rendering the sensor more vulnerable to bulk damage by non-ionizing radiation especially to levels important at LHC [6], [7]. The low resistivity of the Si substrate in standard CMOS processes (typically about  $10 \Omega\text{-cm}$ ) only allows the creation of a very small depletion layer formed around the charge collecting p-n junction. Attempts have been made [8] using epitaxial layers of a few  $\mu\text{m}$  high purity silicon to allow more charge to be collected. Some CMOS technologies allow using high voltage through which the silicon substrate can be depleted by  $\sim 10 \mu\text{m}$  [9], but the rest of the silicon remains undepleted. In this paper we report on an implementation of an advanced MAPS concept employing full CMOS (NMOS and PMOS) electronics in the active area of pixels using a high resistivity (detector-grade) silicon substrate depleted by a bias voltage. The technology is introduced and the performance of a test chip EPCB01 which contains different circuit variants is characterized with respect to analog performance and tolerance to ionizing radiation.

# 2 Test chip EPCB01

To investigate the concept of the DMAPS pixels and their applicability in high energy physics, a prototype chip - EPCB01 has been designed, fabricated and tested. The fabrication process is a 150 nm CMOS process using a high resistivity n-type silicon substrate. The chip itself has been thinned down to a thickness of  $50 \mu\text{m}$ . A schematic cross section of a DMAPS pixel is shown in figure 1.

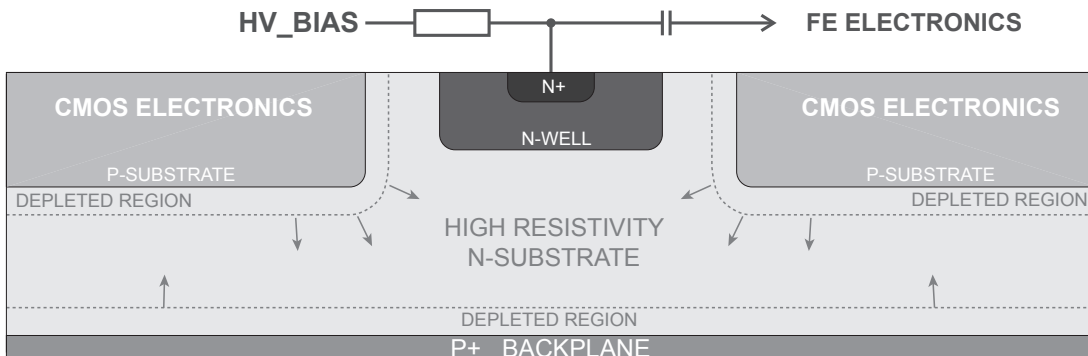


Figure 1: Cross section of the DMAPS pixel.

A deep p-well is implanted in the n-type high resistivity substrate forming a p-substrate for the integration of the CMOS electronics. Transistors are contained within deep n-well which

allows setting of the p-substrate potential independently of CMOS electronics. The sensitive elements are implemented by n-wells implanted in the high resistivity n-type substrate. Although these n-wells (charge collection electrodes) do not form p-n junctions, they create regions with high electric potential and thus build up an electric drift field in the depleted bulk. The depletion region is formed between the p-substrate and the high resistivity n-substrate and between the p+ backplane and the high resistivity n-substrate (see figure 1). This technology allows biasing of the charge collecting n-wells with high voltage (tested up to 15 V), while the FE electronics operates at 1.8 V. More information about the technology can be found in [10]. The collection electrode collects electrons, which are the preferred charge carriers due to their higher mobility with respect to holes. In theory, if full depletion is achieved, a signal of approximately 4000 e<sup>-</sup> per minimum ionizing particle (MIP) can be collected in this sensor configuration. Advantages of this type of sensor are therefore apparent: large signal, fast signal collection and small sensor capacitance (potentially low noise). Six different pixel arrays with dimensions of 8×8 and 6×8 pixels have been integrated in the EPCB01. These arrays differ by architecture of the FE electronics, biasing, coupling and geometry of the sensitive elements.

### 3 DMAPS pixel

A single DMAPS pixel implemented in the EPCB01 can be divided in three sections: 1. high-resistive collection part biased with high voltage, 2. analog FE electronics and 3. digital logic for pixel configuration and read-out. Micrograph of EPCB01 and layout of one DMAPS pixel with highlighted functional blocks is shown in figure 2. The pixel size is 40×40 μm<sup>2</sup> and the sensitive part occupies 25% of the total pixel area. The circuitry inside a pixel contains about 160-180 transistors (depending on the variant, see table 1).

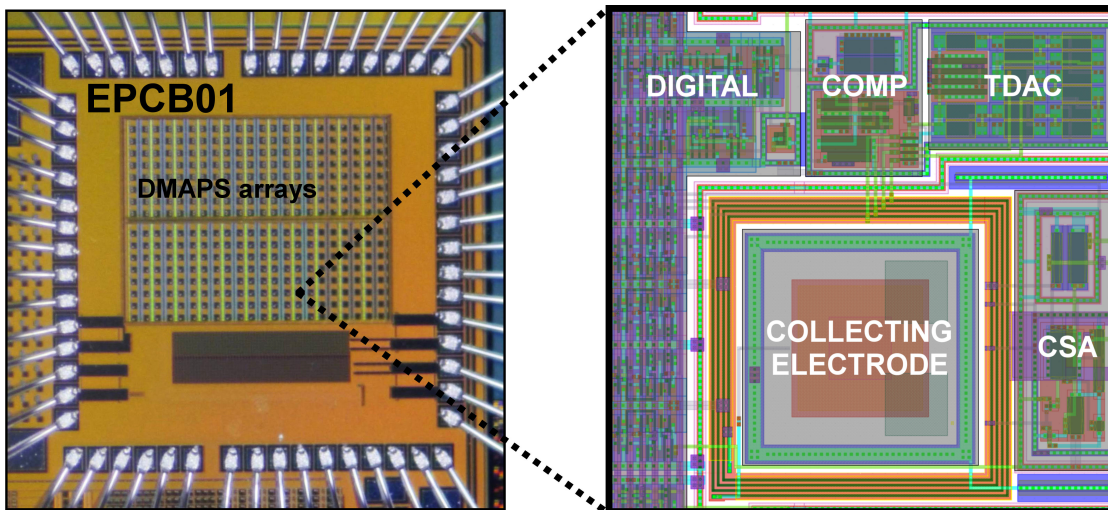


Figure 2: Micrograph of EPCB01 and layout of a single DMAPS pixel.

The analog pixel FE electronics follows a similar scheme as the FE electronics commonly used in hybrid pixel detectors. The analog part contains a Charge Sensitive Amplifier (CSA), a discriminator with a DAC (TDAC) for threshold equalization. Two different architectures of the analog FE electronics have been implemented - (time) continuous and switched. The continuous architecture uses a CSA with a continuous current source feedback followed by standard (time-continuous) discriminator. The switched architecture uses a CSA with a switched feedback and a clamp-and-sample circuit followed by a dynamic discriminator. Motivation for implementation

of the clamp-and-sample circuit is reduction of the low frequency component of the noise. Resetting of the CSA, clamping and sampling is synchronous with a clock frequency of 1 MHz in contrast to the continuous variant. The digital part stores the configuration data for the analog part and enables the read-out of the pixel matrix. The pixel has binary resolution and read-out is implemented through a shift register. Different variants of the DMAPS pixel matrices are labeled V1-V6 and they are described in table 1. A simplified schematic of each variant is shown in figure 3.

Pixel variant	Biasing	Coupling	FE architecture	Matrix dimensions
V1	resistor	AC	continuous	$8 \times 8$
V2	diode	AC	continuous	$8 \times 8$
V3	CSA feedback	DC	continuous	$6 \times 8$
V4	switched	DC	switched	$6 \times 8$
V5	diode	AC	switched	$8 \times 8$
V6	resistor	AC	switched	$8 \times 8$

Table 1: Different variants of the DMAPS pixel matrices implemented in EPCB01.

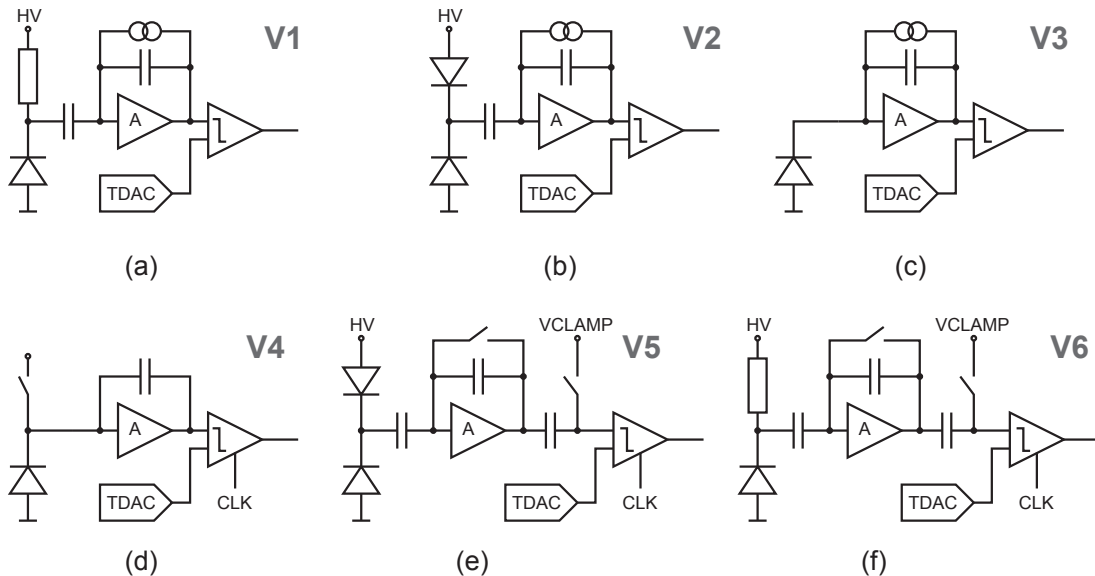


Figure 3: Six different variants of FE electronics V1-V6 shown in figures (a-f) are implemented in EPCB01.

## 4 Performance of the EPCB01 prototype chip

The (analog) performance of the DMAPS pixels is studied by an external charge injection with an in-pixel 2 fF injection capacitor as well as with radioactive sources  $^{90}\text{Sr}$  and  $^{55}\text{Fe}$ .

### 4.1 Gain determination with charge injection

All pixel matrices except V4, which does not contain an injection capacitor, have been examined by external charge injection. A high bias voltage of 11 V has been connected to the collection

electrodes, keeping them depleted during the measurements. P-substrate and the chip backplane have been biased with small negative voltage of -1.5 V. The best analog performance has been achieved with the matrix V2, which will therefore be the design variant on which we focus for the rest of the paper. In general, the pixel variants with a continuous rather than a switching circuit architecture have better performance than the switched variants. The switched variants suffer from a large "kick-back" caused by the dynamic discriminator. When the discriminator samples the signal, the clamping capacitor is discharged by a large amount of parasitic charge injected from the discriminator. This discharge is non-linear. It depends on the signal amplitude. In addition, the clamping capacitor is implemented by a MOSCAP capacitor, which is non-linear as well. Figure 4 shows the gain of the FE electronics as a function of the injected electric charge. Each point represents a mean gain of all pixels of the particular pixel matrix and its error bar represents a standard deviation of the gain arising from gain variation from pixel to pixel. The error bars have been down-sized by a factor of 2 to keep the graph readable.

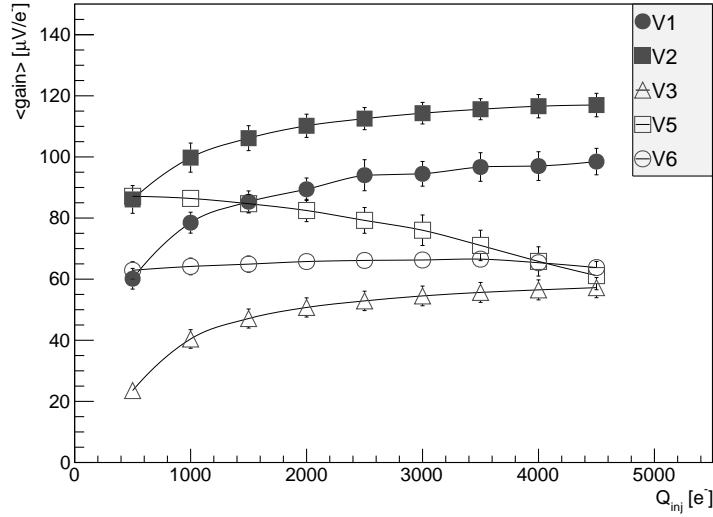


Figure 4: Mean gain of the FE electronics integrated in DMAPS pixels. Size of the error bars has been scaled down by factor of 2.

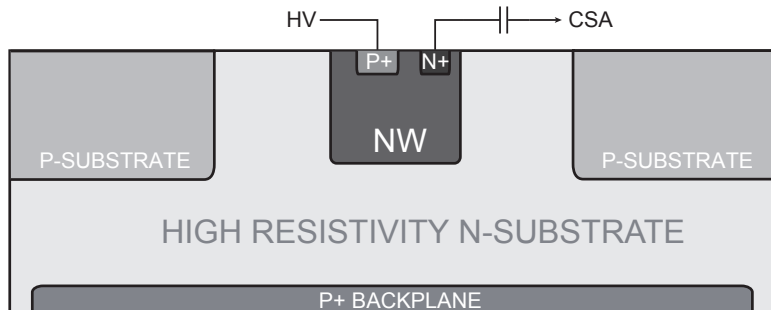


Figure 5: Cross section of the collection electrode used with diode biased pixel variants (V2 and V5).

The highest gain of  $99.8 \mu V/e^-$  measured after the injection of  $1 ke^-$  (typical operating threshold) has been achieved with the pixel matrix V2. The gain dispersion due to electronic mismatch

within matrix variant V2 is  $19.1 \mu\text{V}/e^-$ . Particularly interesting is the comparison of the matrices V1 and V2. The FE electronics in both matrices is identical (including the layout). The shape of the gain dependence on the injected charge (gain curve) is similar in both cases, but they are shifted by  $20.5 \mu\text{V}/e^-$  on average. The gain shift most likely emerges due to the different capacitances of the collection electrodes used in these pixel variants. A schematic cross section of the collection electrode used with diode biased variants is shown in figure 5. Design of the collection electrode used with resistor biasing has been provided by the foundry after design submission and we do not have access to the exact layout parameters. However, if the design of this collection electrode contains wider n-well or n+ diffusion with respect to the collection electrode using diode biasing, this effect may easily increase capacitance of the collection electrode. The CSA uses a common source stage with a relatively small open loop gain of about 76 in the all pixel variants. Therefore the closed loop gain is sensitive to the sensor capacitance. Even greater shift in gain has been observed in case of V3 with respect to V2. The collection electrode in V3 is DC coupled to the FE electronics and is biased by a voltage of about 370 mV provided by CSA feedback. The collection electrode is not fully depleted at this voltage. Therefore the capacitance is even higher than in V1 and the gain is therefore smaller. Almost the same shifts of the gain-curves have been observed in case of V5 and V6 (at the beginning of their dynamic range). However, the character of the non-linearity of the switched variants is different with respect to the continuous variants. The gain-curves of V5 and V6 are not equidistant and the reason for this behavior is not clear.

## 4.2 Noise performance

The noise performance of the DMAPS pixels has been determined by threshold scans and s-curve fits and evaluated in terms of Equivalent Noise Charge (ENC). ENC as a function of injected charge is displayed in figure 6.

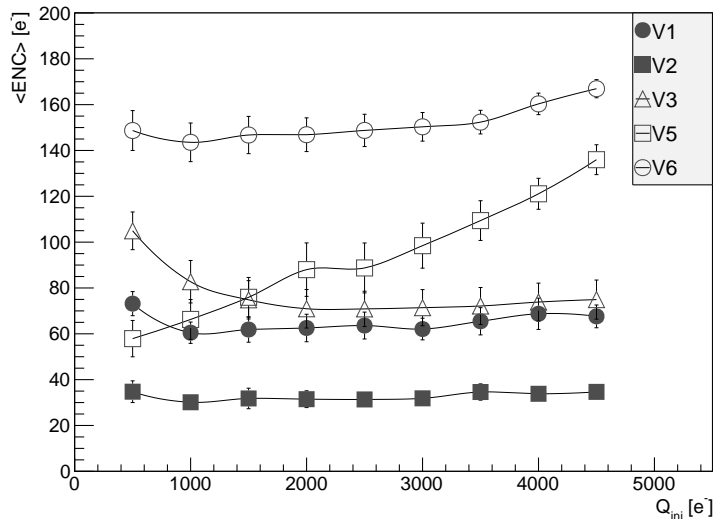


Figure 6: Mean ENC of the FE electronics integrated in the DMAPS pixels. Size of the error bars has been scaled down by a factor of 2.

The lowest noise has been measured with the matrix V2. The differences of the ENC-curves of the matrices V1, V2 and V3 can be attributed to the differences of the sensor capacitance. Each of the switched variants behaves differently in terms of noise. For small signals, the noise

of V5 is comparable with its continuous counterpart (V2) and increases with increasing signal, because at the same time the gain decreases. The noise of variant V6 is much higher than in case of V5. Random Telegraph Signal noise (RTS) represents a significant noise component at all variants of the DMAPS pixels in EPCB01. Spikes of the RTS noise superimposed on the signal from a DMAPS pixel is shown in figure 7. RTS noise is not speciality of EPCB01 only. RTS noise often appears in monolithic pixels as described for example in [11], [12] and certain precautions have to be made in the design to minimize its effect.

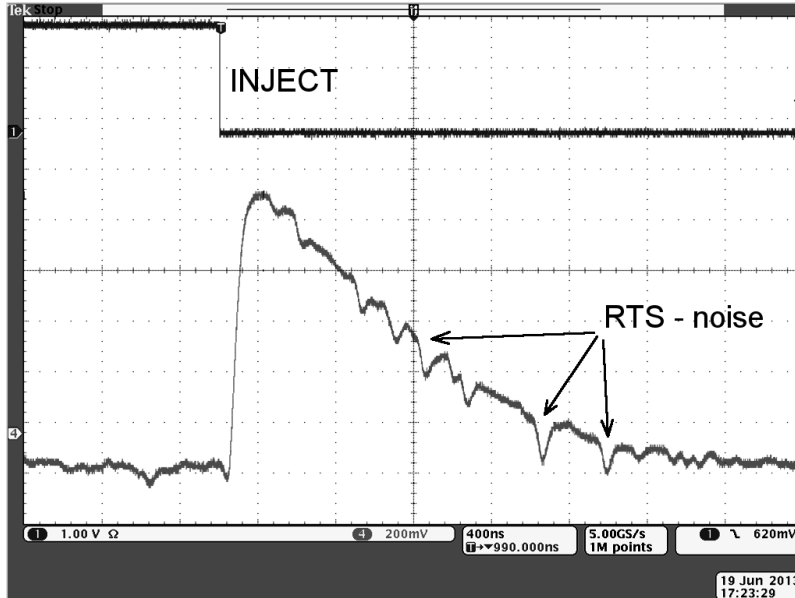


Figure 7: RTS noise observed at the analog output of the DMAPS pixel.

### 4.3 Threshold dispersion

Applications in high energy physics often require a uniform detection threshold across the pixel matrix. Dispersion of the threshold originates from the fabrication process variations and mismatch of the integrated electronic components. Two effects are responsible for the threshold dispersion. The first is the dispersion of the quiescent voltage at the output of the CSA (baseline dispersion) and the second effect is the dispersion of the voltage offset of the discriminator. Each DMAPS pixel contains a 4-bit DAC (TDAC) allowing threshold equalization. The implementation of the TDAC is different in the continuous variants (V1, V2 and V3) and in the switched variants (V4, V5 and V6). The continuous variants use a resistive TDAC embedded in a source follower as shown in figure 8 (a). The advantage of this solution is the possibility to adjust the threshold tuning range if needed. However, the output voltage of the TDAC is not a linear function of the input voltage, resistors occupy a large area in the pixel and the entire TDAC consumes an additional power. The switched variants use a two stage dynamic discriminator. The input voltage offset of the dynamic discriminator is very sensitive to the capacitance of the routing. This fact has been used in the design of a switched capacitance TDAC as shown in figure 8 (b). By adjusting the capacitance between two branches of the discriminator, the voltage offset (discriminating threshold) can be adjusted. This TDAC does not introduce non-linearity to the threshold setting. In addition, this TDAC is very compact in the pixel layout and does not increase the power budget of the pixel.

Both variants of the TDAC have been proven to significantly reduce the threshold dispersion. The distributions of a  $1\text{ ke}^-$  threshold setting before and after tuning of pixels of variants V2 is

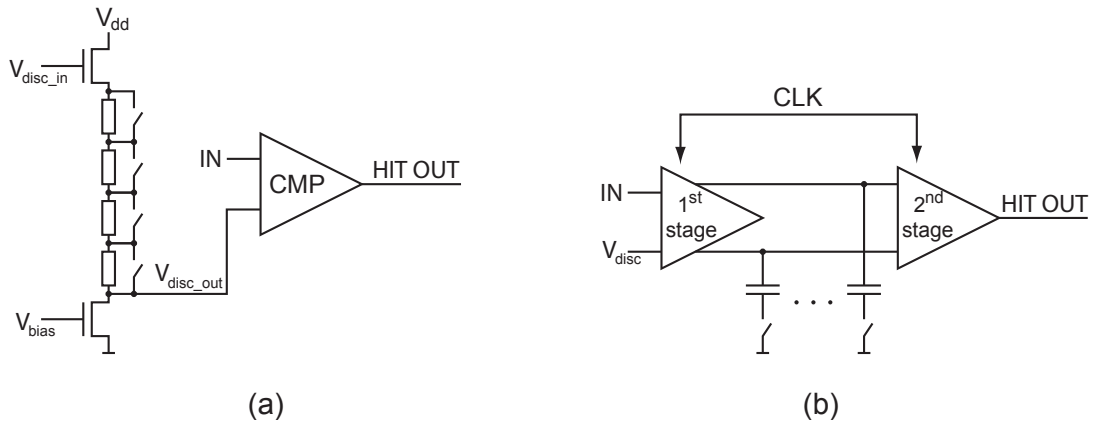


Figure 8: Two different variants of a discriminator with TDAC have been used in EPCB01. A continuous discriminator with resistive TDAC (a) and dynamic discriminator with switched capacitors TDAC (b).

shown in figure 9 (a,b) and threshold dispersion of variant V5 is shown in figure 10 (a,b).

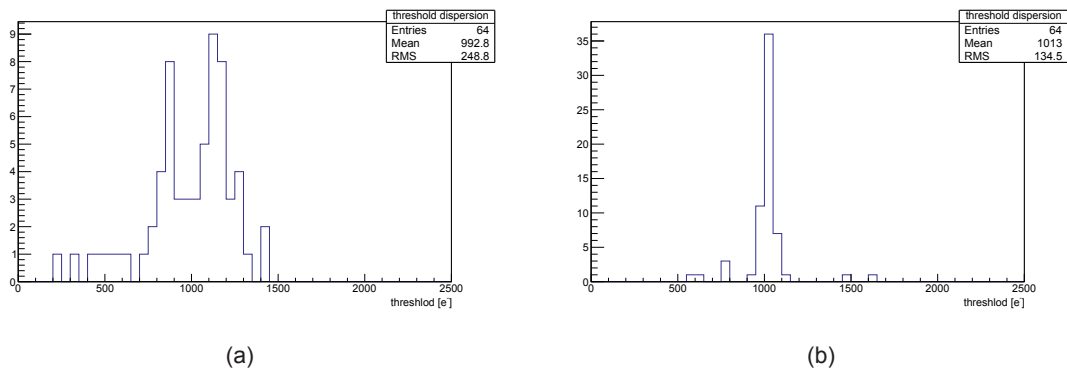


Figure 9: Threshold dispersion of the DMAPS pixels of variant V2 before (a) and after threshold tuning (b).

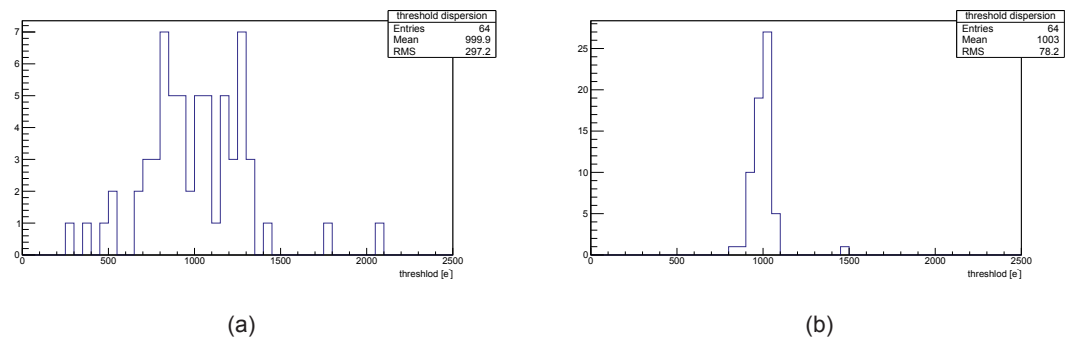


Figure 10: Threshold dispersion of the DMAPS pixels of variant V5 before (a) and after threshold tuning (b).



#### 4.4 Cluster size measurement

In a fine-pitch pixel sensor, the signal charge originating from an ionizing particle diffuses on its path to the electrode. The signal charge can be collected by a cluster of neighboring pixels, the size of which depends on the depleted thickness of the traversed sensor. The cluster size is measured using the DMAPS pixels upon radiation from a  $^{90}\text{Sr}$  radioactive source. The cluster analysis has been performed with the DMAPS pixel array of V2 at several sensor bias voltages (HV\_BIAS). The detection threshold has been adjusted to  $1\text{ ke}^-$  and has been equalized over the matrix. Distributions of the cluster size measured at bias voltages of 2 V and 11 V are shown in figure 11. By comparing these distributions, we can see that at 2 V bias voltage, 29% fewer events are recorded than with a bias voltage setting of 11 V. Events from  $^{90}\text{Sr}$  are predominantly single pixel clusters. However, double pixel clusters become more pronounced at 11 V than at 2 V. This can be explained by assuming that at a higher bias voltage a larger sensor volume is depleted and the total charge spreading by diffusion becomes larger. Consequently, a larger cluster size results.

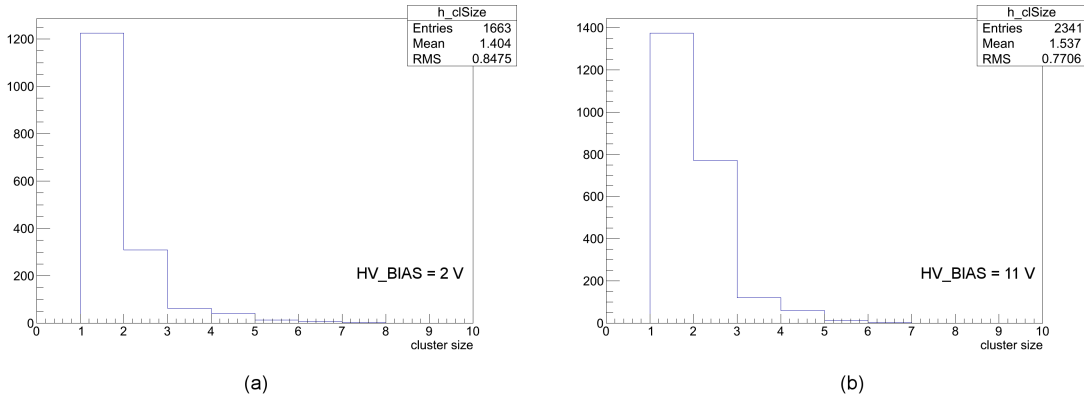


Figure 11: Distribution of the cluster size measured with the DMAPS matrix of variant V2 biased with 2 V (a) and 11 V (b).

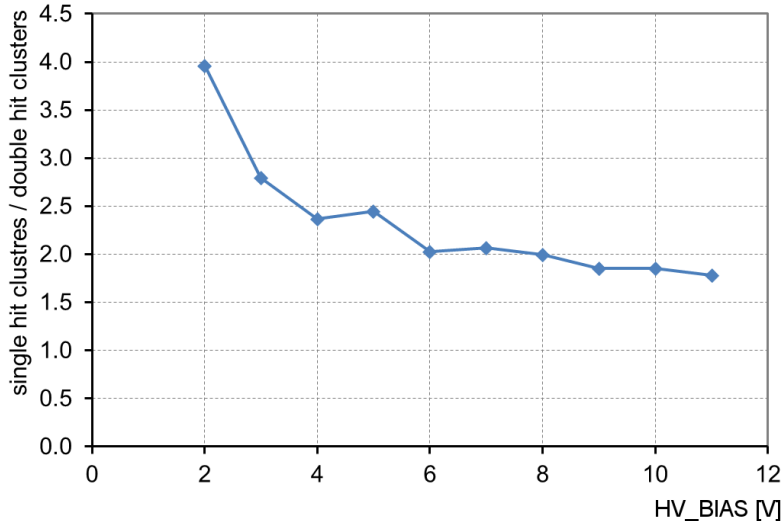


Figure 12: Ratio of the single pixel and double pixel clusters.

Figure 12 shows the ratio of single to double pixel clusters as a function of the sensor bias voltage. This ratio decreases with increasing sensor bias voltage and saturates at a voltage of

about 6 V, while the event rate does not increase beyond this point. At a voltage of 6 V and above the sensor does not collect any more charge and the cluster size ratio remains constant. This, we conclude, indicates full depletion of the sensor.

#### 4.5 Gain determination with $^{55}\text{Fe}$

The response of the pixel FE electronics should not (in ideal case) depend on whether the signal comes from an external charge injection circuit or from the collection electrode. To verify this, an independent measurement of the gain of the pixel FE electronics using an  $^{55}\text{Fe}$  source has been performed. This source emits gamma rays with a characteristic peak in the energy spectrum at 5.9 keV, which translates into a signal of 1640 electrons. The energy of this peak has been measured by each pixel and the gain of the FE electronics has been determined. The same procedure has been completed with an external charge injection of signal of 1640 electrons.

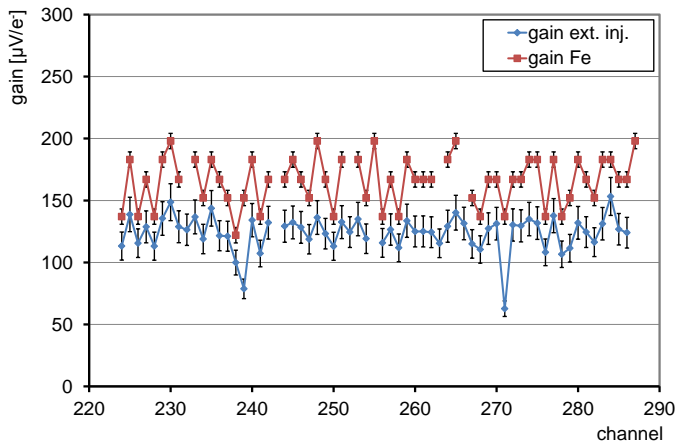


Figure 13: Gain of the FE electronics of each pixel of the matrix V2 determined independently by an external charge injection ( $\langle\text{gain}\rangle=124 \mu\text{V}/e^-$ ) and by radioactive source  $^{55}\text{Fe}$  ( $\langle\text{gain}\rangle=166 \mu\text{V}/e^-$ ).

Gain of each pixel of V2 determined by both methods ( $^{55}\text{Fe}$  irradiation and charge injection) is shown in figure 13. Two effects can be seen: 1. the gain fluctuations determined by  $^{55}\text{Fe}$  are strongly correlated with those seen when the signal was provided by the external charge injection. This result indicates that the gain fluctuations between pixels are predominantly caused by the gain fluctuations of the FE electronics rather than by a non-uniform charge collection efficiency of the collecting electrodes. 2. the mean gain determined by  $^{55}\text{Fe}$  is on average by 34% higher than the mean gain determined by the charge injection. This effect has been studied in detail by design simulations and is most likely caused by the parasitic capacitance of the charge injection circuit and that of the capacitor coupling the collection electrode and electronics.

## 5 Radiation tests

Radiation tolerance of the test chip EPCB01 has been investigated with irradiation from an X-ray tube with end-point energy of 60 keV. The irradiation has been performed within several steps achieving a total ionizing dose of 50 Mrad. After each irradiation period, the chip has been an-

nealed for 100 minutes at 80 °C. Several tests of the analog and digital part of the pixels have been performed after each irradiation period. Radiation induced effects have only been observed in the analog part of the FE electronics. The most sensitive node of the analog part of the DMAPS pixel is the NMOS feedback transistor in the CSA. Radiation induced shift of the threshold voltage of the feedback transistor changes the discharge time of the CSA. The greatest difference of the discharge time has been observed between an unirradiated state and after the first irradiation period (200 krad), then the discharge time changed only insignificantly up to 50 Mrad as can be seen in figure 14. The X-ray irradiation has an overall impact on the FE electronics in terms of changes of gain and noise level of the DMAPS pixels. The dependence of these parameters on the level of irradiation is shown in figure 15 (a,b). The digital part of the DMAPS pixels has been tested between irradiation periods by writing the test data patterns in the configuration shift register and reading them back. No difference has been observed in the data patterns passing the configuration register of the irradiated EPCB01.

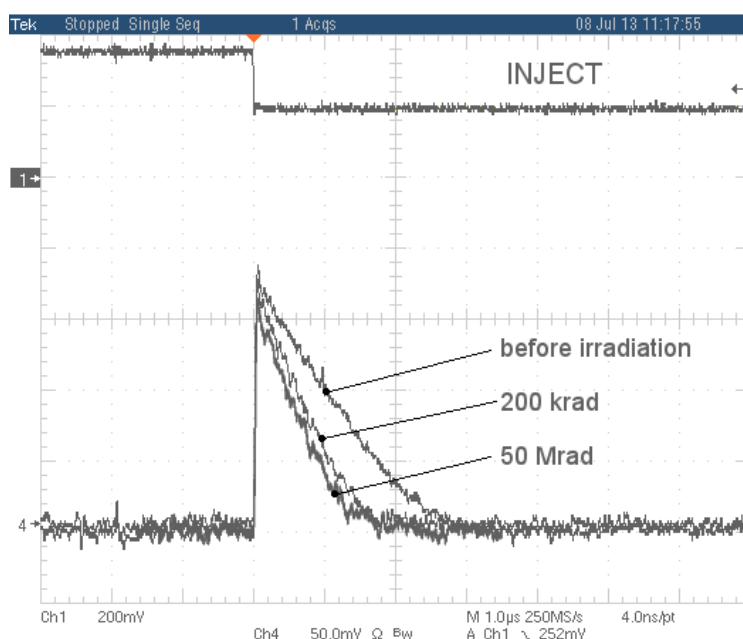


Figure 14: Signal pulse at the output of the CSA (V2) shortens after irradiation.

An additional radiation studies have been performed on an array of individual NMOS and PMOS transistors which is part of EPCB01. All transistors in the array have constant channel length of 150 nm but variable channel width. The NMOS transistor with channel width of 3070 nm has enclosed layout geometry while all other transistors have standard layout. Radiation induced shift of threshold voltage has been observed as well as degradation of transconductance of the transistors. Both results are shown in figure 16 (a,b). Threshold voltage of both transistor types shifts by less than 30 mV within the range of radiation dose. Maximum transconductance of the NMOS transistors degrades by less than 2% and in case of PMOS transistors transconductance degrades by less than 15%. In general, the radiation effects are more significant in small channel width transistors.

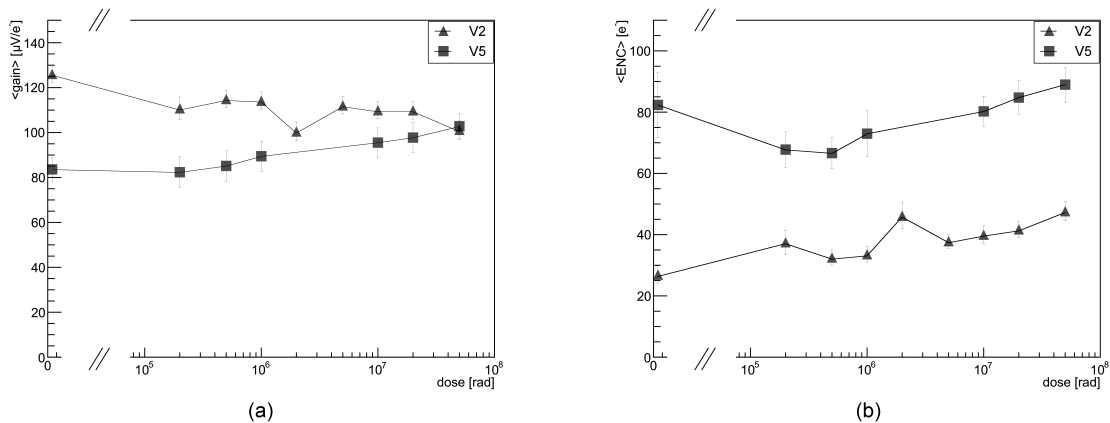


Figure 15: Gain (a) and noise (b) of the DMAPS pixels as a function of X-ray radiation dose. Error bars have been reduced by factor of 2.

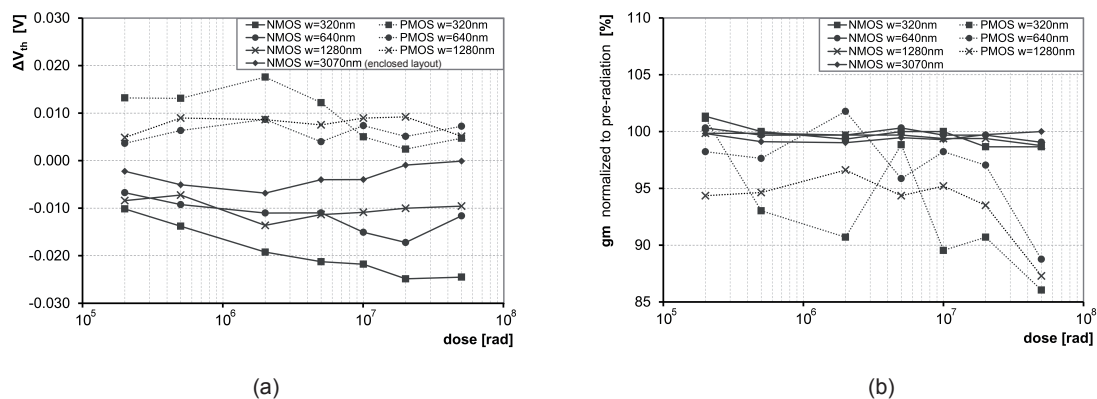


Figure 16: Threshold voltage shift  $\Delta V_{th}$  (a) and transconductance (b) of MOSFET transistors as a function of total ionizing dose. Transistors differ by channel width  $w$  while channel length remains constant (150 nm).

## 6 Summary

A novel concept of Depleted Monolithic Active Pixel Sensors (DMAPS) has been introduced. DMAPS pixels integrate a complex "hybrid pixel like" CMOS electronics and simultaneously benefit from a fully depleted sensor within the same substrate. A commercial CMOS process has been used for fabrication of a prototype DMAPS chip - EPCB01. First tests indicate good functionality of this detector concept, while there is ample room for improvement of the FE electronics. The best performance has been achieved with an AC coupled diode biased collection electrode connected to the time-continuous FE electronics. The gain is  $\sim 100 \mu V/e^-$ , the noise is  $\sim 30 e^-$  with a discharge time of about  $1 \mu s$ . The threshold dispersion after equalization is  $135 e^-$ . The RTS noise has been observed in all variants of the DMAPS pixels and most likely emerges from fluctuations of current of close to minimum size transistors used in the FE electronics. The depletion voltage of the high resistivity substrate has been determined by the means of cluster size saturation to be approximately 6 V. Small radiation effects have been observed in the performance of the analog FE electronics after absorbing the X-ray radiation dose of 50 Mrad. More measurements need to be done to fully understand the DMAPS pixels. In particular, laser scans are needed to determine the position dependence of the charge collection efficiency and more radiation test are needed to learn about the radiation effects in the charge

collecting part. However, important lessons have already been learned during the design and testing of the EPCB01 and they will be addressed in the next generation of the DMAPS test chip.

## 7 Acknowledgement

Authors would like to thank to E. Marchesi and M. Popp from ESPROS Photonics AG for providing information about their technology. Another thanks belong to C. Marinas from Bonn for organization of radiation tests and to T. Müller, H. J. Simonis and S. Heindl from Karlsruhe Institute of Technology for allowing us to perform X-ray irradiation of our chip at their laboratory. At last but not least we would like to thank to W. Dietsche and W. Ockenfels for wire-bonding the test-chips.

## References

- [1] G. Meynants, B. Direcks and D. Scheffer. CMOS active pixel image sensor with CCD performance. *SPIE*, vol. 3410, 1998.
- [2] R. Turchetta et al. A monolithic active pixel sensor for charged particle tracking and imaging using standard VLSI CMOS technology. *Nucl. Instrum. and Meth. A*, vol. 458,(pages 677-689), 2001.
- [3] N. Wermes. Pixel detectors for charged particles. *Nucl. Instrum. and Meth. A*, vol. 604,(pages 370-379), 2009.
- [4] R. Turchetta et al. Monolithic active pixel sensors (MAPS) in a quadruple well technology for nearly 100% fill factor and full CMOS pixels. *Sensors*, vol. 8,(pages 5336-5351), 2008.
- [5] J. Mylroie-Smith et al. First tests of CHERWELL, a monolithic active pixel sensor: A CMOS image sensor (CIS) using 180 nm technology. *Nucl. Instrum. Methods A*, vol. 731,(pages 137-140), 2013.
- [6] ATLAS collaboration. ATLAS pixel detector electronics and sensors. *JINST*, vol. 3,(P07007), 2008.
- [7] CMS collaboration. The CMS experiment at the CERN LHC. *JINST*, vol. 3,(S08004), 2008.
- [8] S. Senyukov et al. Charged particle detection performances of CMOS pixel sensors produced in a 0.18  $\mu\text{m}$  process with a high resistivity epitaxial layer. *Nucl. Instrum. Methods A*, vol. 730,(pages 115-118), 2013.
- [9] I. Perić and C. Takacs. Large monolithic particle pixel-detector in high-voltage CMOS technology. *Nucl. Instrum. Methods A*, vol. 624,(pages 504-508), 2010.
- [10] ESPROS Photonics AG homepage. <http://www.espros.ch>.
- [11] M. Deveaux et al. Random telegraph signal in monolithic active pixel sensors. *IEEE Nuclear Science Symposium Conference Record*, (N49-5), 2008.
- [12] M. Ahoie and S. Kleinfelder. Monolithic sensors for charged-particle imaging using per-pixel correlated double sampling. *IEEE Nuclear Science Symposium Conference Record*, (N05-3), 2006.